The influence of ENSO on global terrestrial water storage using GRACE

T. Phillips,[1,2,3] R. S. Nerem,[1,2,4] Baylor Fox-Kemper,[4,5] J. S. Famiglietti,[6,7] and B. Rajagopalan[4,8]

Received 24 May 2012; revised 12 July 2012; accepted 13 July 2012; published 25 August 2012.

[1] The influence of the El Nino/Southern Oscillation (ENSO) on terrestrial water storage is analyzed for the time period 2003–2010 using monthly estimates of continental water storage from the Gravity Recovery and Climate Experiment (GRACE). Peak correlation between NOAA's Multivariate ENSO Index (MEI) and the measured mass anomaly timeseries shows an R^2 of 0.65 for the Amazon Basin and Borneo in Southeast Asia. By including a Hilbert transformation of the MEI to account for time lag, the R^2 is improved to 0.76. Tropical regions show strong negative correlation with the MEI and arid regions are positively correlated. GRACE is able to detect all the significant known ENSO teleconnection patterns around the globe, including Alaska and Antarctica. In addition, a significant correlation suggests some of Greenland's recent mass loss could be ENSO-related. **Citation:** Phillips, T., R. S. Nerem, B. Fox-Kemper, J. S. Famiglietti, and B. Rajagopalan (2012), The influence of ENSO on global terrestrial water storage using GRACE, *Geophys. Res. Lett.*, *39*, L16705, doi:10.1029/2012GL052495.

1. Introduction

[2] The El Nino Southern Oscillation (ENSO) is a quasi-periodic climate pattern that occurs across the tropical Pacific Ocean at irregular intervals. ENSO is a bi-polar mode characterized by abnormally warm sea surface temperature (El Nino) and cold anomalies (La Nina) in the eastern Pacific [*Trenberth et al.*, 2007]. It has been shown in numerous studies that ENSO has a strong influence on the weather patterns of the Northern Hemisphere [*Hurrell*, 1996; *Trenberth et al.*, 2002], i.e., the severity of forest wild fires in Alaska [*Duffy et al.*, 2005], and temperature variability across much of the United States, including the Rocky Mountains [*Trenberth et al.*, 2002] and as far as the East and the Southeast coastlines [*Alexander et al.*, 2002] are related to ENSO teleconnections. Climatic teleconnections even influence the ice area in the Baltic Sea [*Jevrejeva et al.*, 2003]. In the Southern Hemisphere there is a visible change in precipitation patterns due to ENSO on both sides of the Andes [*Alexander et al.*, 2002] and Australia. The monsoon in Bangladesh and India is also affected by ENSO variability [*Kumar et al.*, 1999]. ENSO teleconnections have been suggested to be the largest linked atmospheric domino effect in annual weather conditions [*Trenberth et al.*, 2002]. Here we investigate terrestrial water storage variability as mass anomaly on the continents using data from the Gravity Recovery and Climate Experiment (GRACE) mission, by comparison to NOAA's Multivariate ENSO Index (MEI) (http://www.esrl.noaa.gov/psd/enso/mei/). We use the terms terrestrial or continental water storage to represent all of fresh water stored on land as snow, ice, surface water, soil moisture and groundwater [*Rodell et al.*, 2004].

[3] The terrestrial water storage $M(t)$ as a function of time at any given location is the difference between precipitation P as mass input minus evaporation E, runoff R and the water storage at a previous time step (t-1). The units are in cm water equivalent height:

$$\mathrm{M(t)} = \boldsymbol{M}(\mathrm{t}-1) + (\mathrm{P}-\mathrm{E}-\mathrm{R}) \quad (1)$$

Numerous publications have analyzed the influence of ENSO on precipitation patterns in various locations [*Kumar et al.*, 1999; *Alexander et al.*, 2002; *Wolter and Timlin*, 2011]. The availability of terrestrial water directly impacts evaporation and runoff. Hence all three variables are influenced by ENSO. We expect that the phase of ENSO will affect the likelihood of precipitation and evaporation, rather than individual weather events. We therefore assume that anomalies in the MEI index directly influence the total terrestrial water storage and hence cause anomalies, described as the monthly mean in equation (1). Therefore we compare the change of the MEI to the continental water storage variability over time to estimate the influence of ENSO. It is also expected that different phases of ENSO may have different effects in different regions; the Hilbert transformation of the MEI is used to estimate the appropriate time lag from extreme MEI values for each region efficiently.

2. Data

[4] We use the GRACE RL04 data for 2003–2010 from the University of Texas Center for Space Research (CSR). We also repeated the analysis with the GeoForschungsZentrum

[1]Department of Aerospace Engineering, University of Colorado at Boulder, Boulder, Colorado, USA.
[2]Colorado Center for Astrodynamics Research, University of Colorado at Boulder, Boulder, Colorado, USA.
[3]Earth System Observation Center, University of Colorado at Boulder, Boulder, Colorado, USA.
[4]Cooperative Institute for Research in Environmental Science, University of Colorado at Boulder, Boulder, Colorado, USA.
[5]Department of Atmospheric and Ocean Sciences, University of Colorado at Boulder, Boulder, Colorado, USA.
[6]Center for Hydrologic Modeling, University of California, Irvine, California, USA.
[7]Department of Earth System Science, University of California, Irvine, California, USA.
[8]Department of Civil, Environmental and Architectural Engineering, University of Colorado at Boulder, Boulder, Colorado, USA.

Corresponding author: T. Phillips, Department of Aerospace Engineering, University of Colorado at Boulder, Boulder, CO 80309, USA. (Thomas.Phillips@colorado.edu)

0094-8276/12/2012GL052495

(GFZ Potsdam) GRACE data and found virtually identical results. The GRACE mission has produced monthly estimates of Earth's gravity field since 2002 [*Tapley et al.*, 2004], which can be used to infer changes in mass at and below the Earth's surface [*Wahr et al.*, 1998]. Numerous studies have been performed to quantify changes in land hydrology, including total terrestrial water storage [*Wahr et al.*, 2004; *Seo et al.*, 2006], evapotranspiration [*Rodell et al.*, 2004], discharge [*Syed et al.*, 2009], groundwater [*Yeh et al.*, 2006], surface water [*Frappart et al.*, 2008] and alpine glacier variability [*Tamisiea et al.*, 2005] from the GRACE data. As the length of the GRACE observational record length increases, inter-annual variations in hydrologic extremes including flooding [*Reager and Famiglietti*, 2009] and drought [e.g. *Yirdaw et al.*, 2008], can also be characterized. Typically, the temporal and spatial resolution of GRACE is viewed as 30 days and 400 km, respectively [*Wahr et al.*, 1998], though smaller temporal and spatial scales can be recovered in some regions. The monthly gravity field is comprised of a set of spherical harmonics (Stokes) coefficients, complete to degree and order 60. The GRACE data have two shortcomings that must be compensated for by the user: substantial noise in short wavelength components (high degree Stokes coefficients), and correlations among coefficients of a fixed order and the same parity of degree [*Wahr et al.*, 1998]. We use the *Swenson and Wahr* [2006] method to remove correlated errors (destriping), and suppress short wavelength noise by applying a Gaussian averaging radius of 250 km to our solutions. These two processes can have the undesired effect of suppressing or removing real gravity signal.

[5] We use the monthly surface mass estimates, which include the atmospheric variability and the ocean mass variation removed (RL04 GSM dataset) for January 2003–December 2010 for the continents. The monthly anomalies, S(x, y, t), (x = latitude, y = longitude) are calculated as the difference from mean mass, $\overline{\mathrm{M}}$, over the 96-month timeseries at each grid node.

$$\mathrm{S(x,y,t)} = \boldsymbol{M}(\mathrm{x,y,t}) - \overline{\mathrm{M}}(x,\mathrm{y}) \tag{2}$$

M(t) is the actual mass measured by GRACE at time t at the location. The mass variations observed for each individual month can therefore be primarily attributed to solid and liquid fresh terrestrial water storage variations. We use NOAA's MEI for the analysis, although other ENSO indices yield similar results. The MEI is the first unrotated principle component of the combined, normalized fields of sea level pressure, zonal and meridional components of wind, surface air pressure and total cloudiness fraction. The units of MEI are standardized and hence a score of 1 represents a full standard deviation departure of the principal component for the respective season involved [*Wolter and Timlin*, 2011].

3. Method

[6] To extract the ENSO influence on terrestrial water storage, multiple corrections to the GRACE data are necessary. We remove the degree 1 zonal coefficients and replace the degree 2 zonal coefficient (C_{20}) - as they reflect changes in the Earth's core rather than at the surface - with coefficients estimated from satellite laser ranging (SLR) estimated coefficients [*Chen et al.*, 2006]. SLR is an effective approach to measuring low degree gravitational changes and has been in use for the last 35 years, particularly for C_{20} [*Chen and Wilson*, 2008; *Nerem and Wahr*, 2011]. The linear rebound of the Earth's surface as an adjustment to the last glaciation is removed. This is a processes referred to as the Glacial Isostatic Adjustment (GIA) [*Paulson et al.*, 2007]. Seasonality induces the largest signal in terrestrial water storage variability. Hence, we remove the annual, semi-annual and secular trend signals to isolate the ENSO signals with w_1 through w_6 being scaling factors.

$$\begin{aligned}\mathrm{S_{detrended}} = S &- \mathrm{w_1} * \sin(2\pi \mathrm{S}) - \mathrm{w_2}\cos(2\pi \mathrm{S}) \\ &- \mathrm{w_3}\sin(4\pi \mathrm{S}) - \mathrm{w_4} * \cos(4\pi \mathrm{S})\end{aligned} \tag{3}$$

To measure the influence of the ENSO on the detrended and deseasonalized GRACE mass anomalies, we perform a least squares fit at each geographic location using a Hilbert transformation of the MEI to estimate the coefficients a, b and c:

$$\begin{aligned}\mathrm{S_{ENSO}(x,y)} = a(\mathrm{x,y}) &+ b(\mathrm{x,y}) * \mathrm{MEI} + c(\mathrm{x,y}) \\ &* \mathrm{imag}(\mathit{Hilbert}(\mathrm{MEI}))\end{aligned} \tag{4}$$

Where the last term is the imaginary part of a Hilbert transform of the MEI, meant to capture terrestrial water storage variations that are out of phase with the MEI. For simplicity we will refer to this function as S_{ENSO}, hence describing the part of S that can be attributed to the influence of ENSO. The Hilbert transformation is a basic tool in Fourier analysis, which shifts each of the sinusoidal Fourier components of the broadband MEI signal by 90 degrees. In the event that there is no lag between the MEI and continental water storage at a given location, c approaches zero [*Salisbury and Wimbush*, 2002] (Figures 1a and 1b).

[7] In a final step we calculate the phase and the amplitude from the coefficients b and c. The amplitude is an estimate of the magnitude of the total influence of the ENSO on terrestrial water storage and the phase allows us to quantify the lag between the ENSO and the continental water storage.

$$\mathrm{AMP} = \sqrt{\mathrm{b}^2 + \mathrm{c}^2} \tag{5}$$

The amplitude is the terrestrial water storage anomaly in $\left[\frac{\mathrm{cm}}{0.1 * \mathrm{MEI} * \mathrm{year}}\right]$. The lag time between the ENSO and the response in terrestrial water storage at the Earth's surface is quantified by calculating the phase:

$$\mathrm{PHASE} = \tan^{-1}\left(\frac{\mathrm{c}}{\mathrm{b}}\right) \tag{6}$$

If PHASE approaches 0, then there is no lag in the response of the terrestrial water storage with respect to the MEI. In the event that PHASE approaches INF, the terrestrial water storage is out of phase with the MEI. In the next section, the results of these calculations are discussed using the b and c coefficients for S_{ENSO} and the PHASE and the amplitude AMP for the influence of ENSO on the continental water storage. In a final step we use the linear Pearson's correlation coefficient to measure the similarity of the terrestrial water anomalies to the MEI.

4. Results

[8] If the c coefficient of the S_{ENSO} is not 0, then a lag between the ENSO signal and the local response in

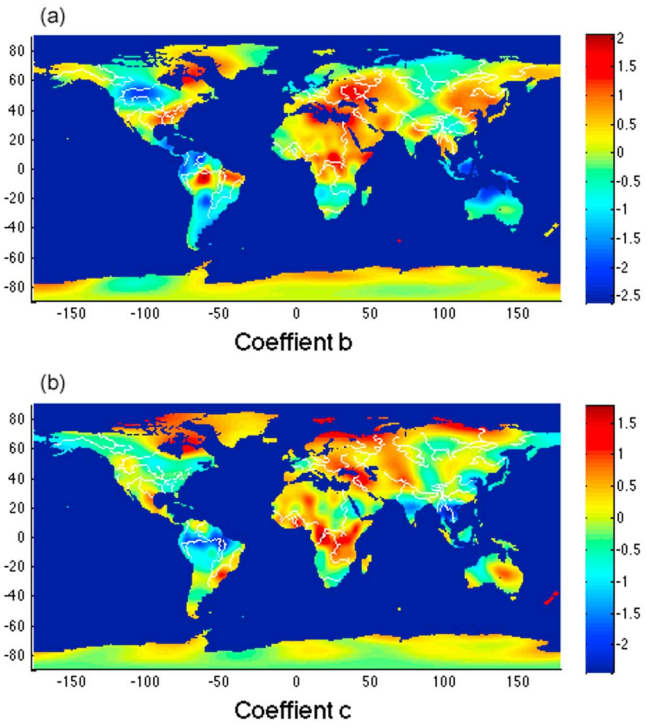

Figure 1. Maps of (a) coefficient b and (b) coefficient c of the Hilbert equation. Higher absolute numbers indicate a higher correlation between MEI and water storage variability. The main river catchments are shown in white.

terrestrial water storage is observed. Hence places such as South America's Amazon basin, Thailand, Alaska, eastern North America and Thule have a lag in response (Figure 1b). We attempt to quantify the time lag between ENSO and the observed terrestrial water storage variability (equation (6)). Venezuela and Papua New Guinea show $c \sim 0$ and large values for coefficient b (Figure 1a): Both have a strong instantaneous response in continental water storage. An average S_{ENSO} for at least 18 1° grid cells is used as a cluster to perform the analysis, as depending on the latitude of the region, a single point would be smaller than the expected GRACE resolution.

[9] Equation (4) was used for a first approximation of the influence of ENSO on the terrestrial water storage changes. In Figure 2a the estimated terrestrial water storage increase in $\left[\frac{\text{cm}}{0.1 * \text{MEI} * \text{year}}\right]$ is shown (water equivalent). With the exception of two regions, all large anomaly values are within the tropics, reaching $20\frac{\text{cm}}{0.1 * \text{MEI} * \text{year}}$ in the Amazon Basin, the Congo Basin and Thailand. The largest negative anomalies are found south of the Himalayas, South America and Northwestern Australia. All of these regions have been identified as being influenced by ENSO in previous publications [*Ropelewski and Halpert*, 1987]. Eastern Antarctica ($7\frac{\text{cm}}{0}.1\text{ME}I$) and Greenland ($6\frac{\text{cm}}{0}.1\text{ME}I$) along its west coast show terrestrial storage variations due to ENSO.

[10] We attempt to quantify the time lag between ENSO and the observed terrestrial water storage variability (equation (6)). The lag map (Figure 2b) shows no clear pattern for the high latitudes, at lower latitudes there seems to be a pattern following the major river basins (compare the Amazon, the Parana or the Orange River in South Africa) (Figure 2b).

[11] We perform a Pearson linear correlation analysis of the GRACE data and the MEI (Figure 3a). Seventeen locations were selected due to their known response to ENSO and are listed in Table 1 including the Koeppen climate classification and the correlation with the MEI variations used in this study. Excluding time lag, the results become significant at 0.21 for a 95% confidence, increasing to 0.26 for the maximum lag included of 3 months. Regions at the Equator and within the Intertropical Convergence Zone (ITCZ) show a negative correlation with the MEI (Venezuela/Colombia (−0.62), Costa Rica (−0.55) in South and Central America, the Indian Subcontinent (−0.45) and Borneo (−0.65) in Southeastern Asia. Regions with high positive correlation are mainly found at latitudes between 20° and 40° (Temperate Zones) such as the Southeastern United States (0.44), the Rio San Francesco in the Northern Region of Brazil (0.34), the Yangtze River (0.45) in China, and the island of Hokkaido (0.51) in East Asia. Additional high positive correlations are found in arid/continental regions such as the Arabian Peninsula (0.23) or the coast of Eastern Antarctica (0.45). There is a high correlation between the west coast of Greenland (0.41) and the MEI.

[12] In a second approach, we correlated the seasonally averaged (3-months) gravity field data with the seasonal MEI (MEI_S) to side step the lag dependency: A three-month average of GRACE mass variation data is compared to a 3 month averaged MEI (Figure 3b). The seasonal map shows better agreement in certain areas (East Antarctica (0.61), the Southeastern United States (0.50), India (−0.55) or Western Greenland (0.41). In central Africa a clear correlation is

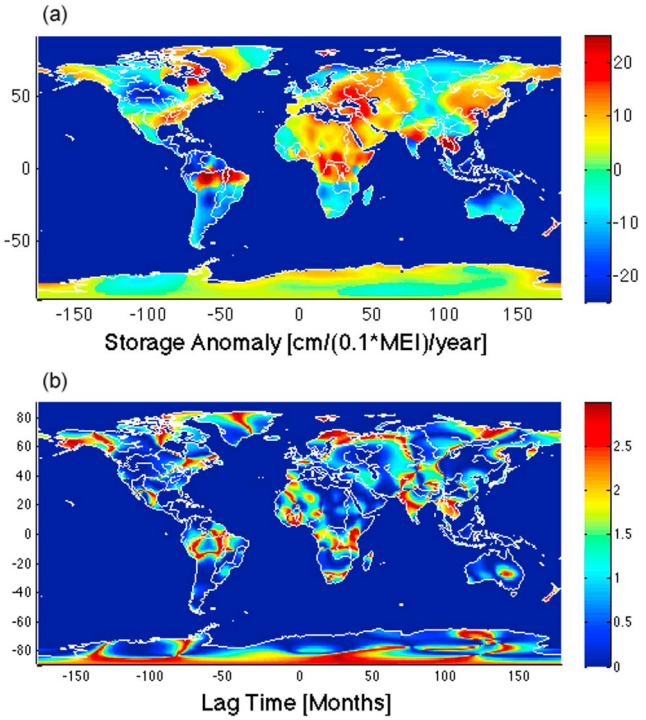

Figure 2. (a) The storage anomalies due to change in S_{ENSO}. The major rivers are shown in white. (b) The lag time in months between ENSO and the observed signal. Major rivers are shown in white.

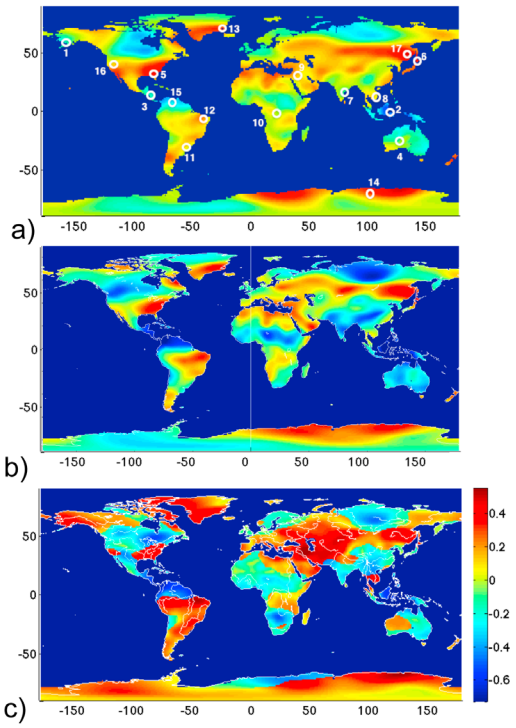

Figure 3. (a) The correlation between the land mass variability and the MEI index for the CSR dataset. This analysis shows the correlation for monthly data. The locations of the 17 regions listed in Table 1 are indicated. (b) The correlation map for MEI_S. (c) Correlation map for S_{ENSO}. The rivers are shown in white.

visible north of the Congo that was non-existent in the MEI-correlation. The correlation decreases, however, for Borneo (−0.60) and Alaska (0.38), or in some cases becomes non-existent (Rio Parana and Rio San Francesco in Brazil).

[13] In Figures 3b and 3c, we show the correlation map for the GRACE monthly gravity fields with the $S_{ENSO}(x, y)$. However, $S_{ENSO}(x, y)$ has been transformed using the MEI and hence is no longer truly independent from the GRACE gravity fields (equation (4)). With the exception of the Congo and the Indian Subcontinent, no location shows a decrease in correlation. Venezuela/Columbia (−0.78), Borneo (−0.76), Alaska (0.63) or Hokkaido (0.61) show much improved correlations. Large water bodies such as the Great Lakes and the catchment areas such as the Rio Grande in North America, the Sanaga and Congo Rivers in Central Africa or the Yangtze River in Northeastern China influence many of these regions.

[14] The timeseries of five sub-regions that show high correlations with the S_{ENSO} are: (i) Venezuela and Central America (Figure 4a) and (ii) Southeastern Asia including Borneo, Sulawesi and Papua New Guinea (Figure 4b); (iii) the Southeastern United States (Figure 4c); (iv) Alaska for the Northern Pacific Ocean (Figure 4d) and (v) East Antarctica for the Southern Pacific Ocean (Figure 4e). The first two figures show strong negative correlations (−0.78 and −0.76), whereas the others show strong positive correlations at 0.52, 0.53 and 0.63 respectively. In Figure 4f we show the geographical locations of the five timeseries discussed here.

[15] Venezuela and Borneo (Figures 4a and 4b) have two distinct features: 1) the agreement between the local GRACE estimate and the S_{ENSO} increases over time until there is a close match starting in 2007 to the present; 2) There are only positive correlations for S_{ENSO}. The S_{ENSO} (blue) switches the MEI (red) in the case of a negative correlation so that it becomes highly correlated with the CSR GRACE terrestrial water storage data (green).

[16] The Southeastern United States (SEUS) shows a positive correlation: The MEI (red) and the $S_{ENSO_{SEUS}}$ (blue) show the same trends (Figure 4c). As the correlation index (0.52) suggests, the agreement is less than in the previous example. The range of variability in the local terrestrial water storage estimate (green) indicates that this region is heavily influenced by ENSO (18 cm). If the time series is smoothed using a Gaussian filter to remove the influence of additional climate variability, the correlation between $S_{ENSO_{SEUS}}$ and the local gravity field variability reaches a correlation of 0.68 (not shown). Alaska shows a high positive correlation and the trend is similar to the Southeastern United States (Figure 4d). The final location described is East Antarctica (EA) (4e), which has a positive correlation with local $S_{ENSO_{EA}}$ (0.63) and the courses show an improved agreement in comparison to the Southeastern United States. In fact if 2008 is excluded, East Antarctica has a similar correlation with the S_{ENSO}, as Borneo (−0.76).

5. Discussion

[17] Large areas in the arid regions (e.g. Arabian Peninsula) show significant correlation between ENSO and the terrestrial water storage. The total storage, and thus fluctuations in storage, in these regions is low, so that both coefficients b and c are small. It is therefore less likely that it is signal rather than noise that is being detected. Hence a robust signal only results when a high correlation with MEI exists and the amplitude is not near zero.

[18] The largest terrestrial water storage anomalies due to ENSO both negative and positive are found between 15°S and 15°N. This is not surprising as the ITCZ experiences a large seasonal precipitation fluctuation (monsoons), and its longitudinal center of precipitation migrates with ENSO phase from the western Pacific during La Nina to the eastern

Table 1. The Various Correlations for the CSR Datasets Between Selected Locations and the MEI, the MEI_S and the S_{ENSO}[a]

Number	Region	Climate	corr MEI	corr MEI_S	corr MEI_H
1	Alaska	Tundra	∼0	∼0	0.63
2	Borneo	Tropical	−0.65	−0.61	−0.76
3	Central America	Tropical	−0.55	−0.52	−0.63
4	Central Australia	Arid	∼0	∼0	0.32
5	South East USA	Temperate	0.44	0.59	0.52
6	Hokkaido	Temperate	0.51	0.54	0.61
7	India	Tropical	−0.45	−0.55	−0.50
8	Indochina	Tropical	∼0	∼0	0.50
9	Near East	Arid	0.23	0.24	0.53
10	Congo	Tropical	∼0	−0.57	0.32
11	Rio Parana	Temperate	∼0	∼0	0.38
12	Rio San Francesco	Temperate	0.34	0.00	0.60
13	Southeast Greenland	Arid/Polar	0.41	0.55	0.55
14	East Antarctica	Arid/Polar	0.49	0.61	0.53
15	Venezuela/Columbia	Tropical	−0.62	−0.63	−0.78
16	Washington	Costal	−0.53	−0.55	∼0
17	Yangtze River	Temperate	0.45	0.5	0.53

[a]The Climate Classification are according to Koeppen is included in column 2 [*Peel et al.*, 2007]. The locations indicated in Figure 4b.

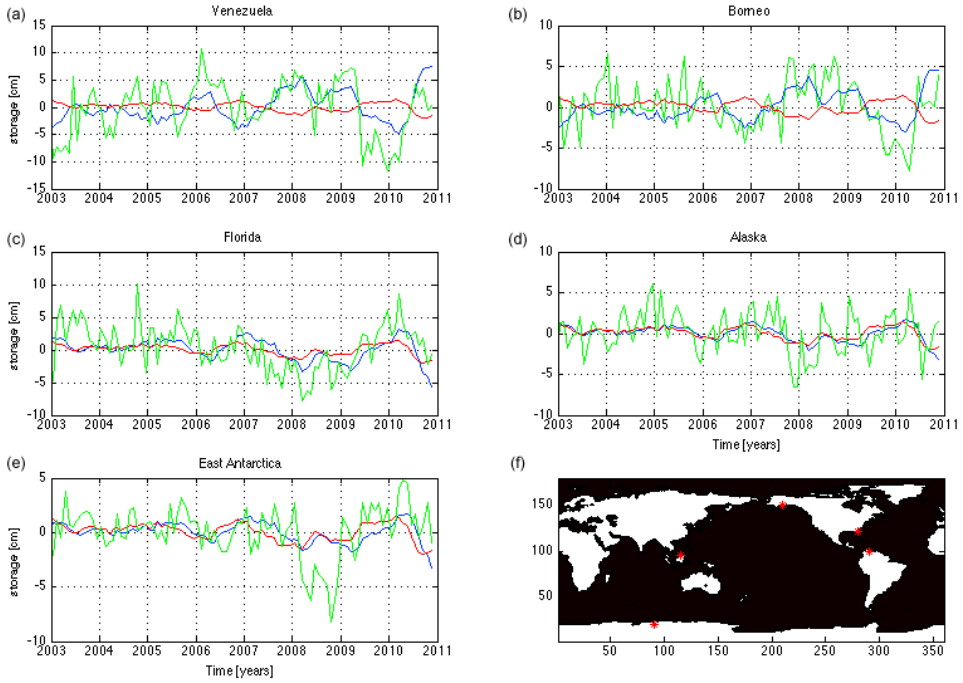

Figure 4. Timeseries for (a) Venezuela, (b) Borneo, (c) South East USA, (d) Alaska and (e) East Antarctica. The MEI is shown in red, the S_{ENSO} in blue, the mass anomaly in green. (f) The location of each of the curves is shown.

Pacific during El Nino. Hence locations such as Borneo, Thailand, North Western Australia, the Indian Subcontinent, the Amazon Basin and Central America show large anomalies. They are all located in the tropical climate zone. The climate in all of these regions is driven primarily by the ITCZ and its seasonal and interannual migrations, other climate patterns weakly influence these regions and hence little noise is introduced. All the named regions are located at the periphery of the Pacific Ocean. Many of the highest anomalies are to be found along rivers, such as the Amazon, the Congo, the Yangtze or the Met Cong (Figure 2a). The river basins collect much of the rainwater and it is therefore to be expected that these regions should show a clear signal with a few months of time lag, as is found in Figure 2b. The largest lags are found along the Amazon, the Orange River in South Africa, the Niger or the Met Kong. More interestingly, the Mackenzie River in Canada shows a strong signal. At higher latitudes the observed signals are less obviously correlated with expected effects, and may be influenced by multiple factors or spherical harmonic artifacts. The South Alaskan Coastal Mountain Range shows a large lag. This could be the result of snow rather than rain that is stored. At the southern foot of the Himalayas in India and in Thailand a large lag exists. This could be the result of irrigation.

[19] The Canadian Archipelago and the west coast of Greenland deserve a brief discussion. Recent studies have shown that glaciers in the Canadian Arctic are losing mass. The melt signal has been increasing along the west coast of Greenland since 2002 as GRACE observations show. During this time period we have seen three strong La Nina years (MEI is negative). Hence the MEI signal has been predominantly negative during this time period. We see a strong positive anomaly for the region indicating mass loss. As a result we see a strong significant correlation for this region with ENSO (Figures 3a–3c): the highest correlation is to be found at the location of the fastest flowing glacier in the Northern Hemisphere: Jakobshavn Isbrae. Is ENSO therefore in part responsible for ice loss seen in this region, or is it a false positive correlation of two covariant but causally unconnected timeseries? The unclear lag signal suggests a causal relationship is improbable. However, other climate indicators such as global mean sea level change also contain ENSO signals [*Hamlington et al.*, 2011]. The degree to which Greenland mass loss can be attributed to ENSO, and the degree to which it may be reversed with ENSO reversals can only be answered with a longer GRACE timeseries.

[20] Regions located in temperate regions between 20° and 40° latitude in Central and Northern Africa show little correlation with the MEI, but more with the MEI_S or the S_{ENSO}. Most of these regions show a positive correlation with MEI. These regions are affected also by the westerly wind systems. Hence this could indicate that the paths of the fronts are in part driven by ENSO as suggested in *Trenberth et al.* [2007]. The increase in strength of the correlation from MEI to S_{ENSO} shows that the response time between ENSO and observed terrestrial water storage anomaly increases with distance to the Central Pacific Ocean. For all discussed locations bordering the Pacific Ocean the correlation is the highest with the S_{ENSO} (Figure 3a).

[21] The MEI_S correlation is in general lower than the MEI and the S_{ENSO} correlations. This is because we find positive correlation further inland and further from the source of the ENSO in the Pacific. The time for the response through the teleconnections increases. The correlation between water storage anomalies and MEI decreases with increasing distance to the location where the MEI is created. Thus, the lag

times are short and stay similar, as there are no continental climate modes and patterns to suppress these teleconnections. This argument is supported in that the Rio Parana and the Rio San Francesco show no correlation for the MEI_S: Both have a similar lag time of 1/2 months that shows a high correlation. However the months before and after show an insignificant correlation with the ENSO. However, the teleconnections are already clearly visible here. High latitude regions and regions at great distance of the Pacific Ocean need to be interpreted with caution due to the interference of other climate oscillations such as the North Atlantic Oscillation (NAO), the Pacific Decadal Oscillation (PDO) or the Arctic Oscillation (AO) [*Wanner et al.*, 2001]. Thus, the probability of false positives at these locations is high, so we don't discuss the high correlation in Siberia.

[22] The results presented here are all based on data from the global coverage of the GRACE satellites and MEI record. Despite the short timespan of available GRACE data we have been able to get remarkably high correlations between the terrestrial water storage and the MEI, the S_{ENSO}, the MEI_S. In using the S_{ENSO} we are able to capture locations that are shifted in their response time. However, there still remains much uncertainty in the lag time, and there are likely to be false correlations in some regions. This uncertainty will decrease as the length of the GRACE dataset increases. The simplicity of this analysis allows us to estimate how much the terrestrial water storage at a certain location will change due to ENSO. Currently, the significant level is questionable due to the shortness of the timeseries and the unclear degree of freedom. In a time series such as the anomalies discussed in this study the independence of each measure is unclear as in the case of mean monthly GRACE values, the timeframe for the mean is at random. A second important issue is to study the best method to measure the influence of ENSO. As this study was pursued on a global scale, a common method was selected. However, there is much indication that the dependency in many regions is not linear as suggested here: Tipping points, only El Nino or La Nina influenced are found. We do however plan to do this in the future.

[23] As the dataset increases, we will be able to do a more robust analysis. In the best-case scenario we will be able to make short-term predictions on how the terrestrial water availability will change and improve flood and draught forecasts significantly by estimating the continental water storage anomaly due to ENSO. We anticipate that these data might also be valuable in validating the interannual variability of precipitation, evaporation, and runoff patterns in climate models.

6. Conclusions

[24] We have estimated the correlation of satellite-observed continental water storage associated with ENSO. This was possible despite the relatively short dataset available (2003–2010). We were able to make a first quantitative estimate of the terrestrial water storage anomaly and the lag time associated with certain teleconnections. The accuracy of these results will improve as the GRACE dataset increases and more ENSO variability is captured.

[25] **Acknowledgment.** This work was supported by the NASA GRACE Science Team and NSF FRG 0855010.

[26] The editor and the authors would like to thank the two anonymous reviewers.

References

Alexander, M. A., et al. (2002), The atmospheric bridge: The influence of ENSO teleconnections on air–sea interaction over the global oceans, *J. Clim.*, *15*, 2205–2231, doi:10.1175/1520-0442(2002)015<2205:TABTIO>2.0.CO;2.

Chen, J. L., and C. R. Wilson (2008), Low degree gravity changes from GRACE, Earth rotation, geophysical models, and satellite laser ranging, *J. Geophys. Res.*, *113*, B06402, doi:10.1029/2007JB005397.

Chen, J. L., and C. R. Wilson, and K.-W. Seo (2006), Optimized smoothing of Gravity Recovery and Climate Experiment (GRACE) time-variable gravity observations, *J. Geophys. Res.*, *111*, B06408, doi:10.1029/2005JB004064.

Duffy, P. A., et al. (2005), Impacts of large-scale atmospheric-ocean variability on the Alaskan fire season severity, *Ecol. Appl.*, *15*(4), 1317–1330, doi:10.1890/04-0739.

Frappart, F., F. Papa, J. S. Famiglietti, C. Prigent, W. B. Rossow, and F. Seyler (2008), Interannual variations of river water storage from a multiple satellite approach: A case study for the Rio Negro River basin, *J. Geophys. Res.*, *113*, D21104, doi:10.1029/2007JD009438.

Hamlington, B. D., R. R. Leben, R. S. Nerem, W. Han, and K.-Y. Kim (2011), Reconstructing sea level using cyclostationary empirical orthogonal functions, *J. Geophys. Res.*, *116*, C12015, doi:10.1029/2011JC007529.

Hurrell, J. W. (1996), Influence of variations in extratropical wintertime teleconnections on Northern Hemisphere temperature, *Geophys. Res. Lett.*, *23*, 665–668, doi:10.1029/96GL00459.

Jevrejeva, S., J. C. Moore, and A. Grinsted (2003), Influence of the Arctic Oscillation and El Nino-Southern Oscillation (ENSO) on ice conditions in the Baltic Sea: Wavelet approach, *J. Geophys. Res.*, *108*(D21), 4677, doi:10.1029/2003JD003417.

Kumar, K. K., et al. (1999), On the weakening relationship between the Indian Monsoon and ENSO, *Science*, *284*, 2156–2159, doi:10.1126/science.284.5423.2156.

Nerem, R. S., and J. Wahr (2011), Recent changes in the Earth's oblateness driven by Greenland and Antarctic ice mass loss, *Geophys. Res. Lett.*, *38*, L13501, doi:10.1029/2011GL047879.

Paulson, A., et al. (2007), Inference of mantle viscosity from GRACE and relative sea level data, *Geophys. J. Int.*, *171*, 497–508, doi:10.1111/j.1365-246X.2007.03556.x.

Peel, M. C., et al. (2007), Updated world map of the Koeppen-Geiger climate classification, *Hydrol. Earth Syst. Sci.*, *11*, 1633–1644, doi:10.5194/hess-11-1633-2007.

Reager, J. T., and J. S. Famiglietti (2009), Global terrestrial water storage capacity and flood potential from GRACE, *Geophys. Res. Lett.*, *36*, L23402, doi:10.1029/2009GL040826.

Rodell, M., J. S. Famiglietti, J. Chen, S. I. Seneviratne, P. Viterbo, S. Holl, and C. R. Wilson (2004), Basin-scale estimates of evapotranspiration using GRACE and other observations, *Geophys. Res. Lett.*, *31*, L20504, doi:10.1029/2004GL020873.

Ropelewski, C. F., and M. S. Halpert (1987), Global and regional scale precipitation patterns associated with the El Niño–Southern Oscillation, *Mon. Weather Rev.*, *115*, 1606–1626, doi:10.1175/1520-0493(1987)115<1606:GARSPP>2.0.CO;2.

Salisbury, J. I., and M. Wimbush (2002), Using modern time series analysis techniques to predict ENSO events from SOI time series, *Nonlinear Processes Geophys.*, *9*, 341–345, doi:10.5194/npg-9-341-2002.

Seo, K.-W., C. R. Wilson, J. S. Famiglietti, J. L. Chen, and M. Rodell (2006), Terrestrial water mass load changes from Gravity Recovery and Climate Experiment (GRACE), *Water Resour. Res.*, *42*, W05417, doi:10.1029/2005WR004255.

Swenson, S., and J. Wahr (2006), Post-processing removal of correlated errors in GRACE data, *Geophys. Res. Lett.*, *33*, L08402, doi:10.1029/2005GL025285.

Syed, T. H., J. S. Famiglietti, and D. P. Chambers (2009), GRACE-based estimates of terrestrial freshwater discharge from basin to continental scales, *J. Hydrometeor*, *10*, 22–40, doi: 10.1175/2008JHM993.1.

Tamisiea, M. E., E. W. Leuliette, J. L. Davis, and J. X. Mitrovica (2005), Constraining hydrological and cryospheric mass flux in southeastern Alaska using space-based gravity measurements, *Geophys. Res. Lett.*, *32*, L20501, doi:10.1029/2005GL023961.

Tapley, B. D., S. Bettadpur, M. Watkins, and C. Reigber (2004), The Gravity Recovery and Climate Experiment: Mission overview and early results, *Geophys. Res. Lett.*, *31*, L09607, doi:10.1029/2004GL019920.

Trenberth, K. E., J. M. Caron, D. P. Stepaniak, and S. Worley (2002), Evolution of El Nino-Southern Oscillation and atmospheric surface temperature, *J. Geophys. Res.*, *107*(D8), 4065, doi:10.1029/2000JD000298.

Trenberth, K. E., et al. (2007), Observations: Surface and atmospheric climate change, in *Climate Change 2007: The Physical Science Basis. Contribution of Working Group I to the International Panel on Climate Change*, edited by S. Solomon et al., pp. 235–336, Cambridge Univ. Press, New York.

Wahr, J., M. Molenaar, and F. Bryan (1998), Time variability of the Earth's gravity field: Hydrological and oceanic effects and their possible detection using GRACE, *J. Geophys. Res.*, *103*, 30,205–30,229, doi:10.1029/98JB02844.

Wahr, J., S. Swenson, V. Zlotnicki, and I. Velicogna (2004), Time-variable gravity from GRACE: First results, *Geophys. Res. Lett.*, *31*, L11501, doi:10.1029/2004GL019779.

Wanner H., S. Brönnimann, C. Casty, D. Gyalistras, J. Luterbacher, C. Schmutz, D. B. Stephenson, and E. Xoplaki (2001), North Atlantic Oscillation - concepts and studies, *Surv. Geophys.*, *22*(4), 321–382, doi:10.1023/A:101421731789.

Wolter, K., and M. S. Timlin (2011), El Nino/Southern Oscillation behavior since 1871 as diagnosed in an extended multivariate ENSO Index (MEI), *Int. J. Climatol.*, *31*, 1074–1087, doi:10.1002/joc.2336.

Yeh, P. J.-F., S. C. Swenson, J. S. Famiglietti, and M. Rodell (2006), Remote sensing of groundwater storage changes in Illinois using the GRACE, *Water Resour. Res.*, *42*, W12203, doi:10.1029/2006WR005374.

Yirdaw, S. Z., et al. (2008), GRACE satellite observations of terrestrial moisture changes for drought characterization in the Canadian Prairie, *J. Hydrol.*, *356*(1–2), 84–92, doi:10.1016/j.jhydrol.2008.04.004.